Lattice dynamics and Raman response of (113) GaAs/AlAs superlattices

P. Castrillo* and L. Colombo
Dipartimento di Fisica, Università di Milano, via Celoria 16, 20133 Milano, Italy

G. Armelles
Centro Nacional de Microelectrónica, Consejo Superior de Investigaciones Científicas (CSIC), Serrano 144, 28006 Madrid, Spain
(Received 28 June 1993; revised manuscript received 20 December 1993)

We present a supercell model calculation of the vibrational properties and Raman response of (113)-oriented GaAs/AlAs superlattices. Phonon-dispersion relations are calculated both along the growth axis and in the normal planes. The angular dispersion of the zone-center optical phonons is calculated as well, and some unusual features are discussed. We also calculate the Raman response in the backscattering geometry: to this aim, the bond polarizability model has been suitably extended to the case of arbitrarily oriented superlattices. The effects of the interface cationic diffusion on the Raman spectra are discussed. A comparison with experimental data is finally presented and discussed.

I. INTRODUCTION

The lattice-dynamical properties of GaAs/AlAs superlattices (SL's) have been widely studied both experimentally and theoretically.[1] The (001)-oriented SL has been used as the paradigmatic system to investigate the mechanisms of acoustical-phonon folding and optical-phonon confinement. Vibrations localized at the interface have been studied as well. The growth of a (001)-oriented heterostructure can be very accurately controlled and high quality SL's can be actually obtained. Moreover, the (001) SL's have a high-symmetry group for the phonon wave vector that prevents any polarization mixing between longitudinal and transverse modes. This feature (together with the selection rules for the Raman scattering in the backscattering configuration) allows for a straightforward interpretation of the Raman spectra.

More recently, good samples of GaAs/AlAs heterostructures have been grown along low-symmetry directions by epitaxial techniques, thus opening the possibility of investigating orientation-dependent vibrational properties. In particular, a detailed study (both theoretical and experimental) has been reported on (110)- and (012)-oriented systems.[2-4]

In this paper, we present a thorough theoretical investigation on the phonon properties and Raman response of (113)-oriented GaAs/AlAs superlattices. The peculiarity of such a system—common to all the (11n)-grown heterostructures other than the (111) ones—is that confined phonons have either pure-transverse polarization (parallel to the [1$\bar{1}$0] direction) or mixed-longitudinal and mixed-transverse character. Another interesting feature is the strong angular dispersion at the Γ point shown by several optical phonons when their (vanishing) wave vector is rotated away from the growth direction. Dispersion is shown by other superperiodic structures as well;[5,6] in the present case, however, it displays an unusual dependence upon the plane in which the phonon wave vector is rotated.

Our investigation is based on the adiabatic bond charge model[7] (BCM) as far as the lattice dynamics is concerned, the mass approximation being adopted for the AlAs layers (i.e., the same parameters have been used in the calculations for both GaAs and AlAs constituents with the exception of the cation mass).[5,8] Details of the dynamical model and the supercell approach used in the present paper are given in Sec. II. We present the dispersion relations of two ultrathin superlattices calculated along the borders of the irreducible SL Brillouin zone (BZ). Angular dispersions are investigated as well. In Sec. III we calculate the Raman response of (113) SL's. The intensity of the Raman scattering is evaluated in the framework of the bond polarizability model[9] (BPM) which has been suitably generalized for an arbitrarily oriented SL (Sec. III A) and explicitly developed for ideal (113) SL's (Appendix A). Calculations for ultrathin superlattices are presented and discussed (Sec. III B). Further, we analyze the effects of the interface disorder on the Raman spectra due to the Ga-Al interdiffusion (Sec. III C). We compare our theoretical predictions to available experimental data in Sec. III D. Finally, some conclusions are drawn in Sec. IV.

II. LATTICE DYNAMICS

A. The model for bulk phonons

The bond charge model has been recently defined as the most reliable and best physically grounded dynamical model for III-V compounds,[10] when compared to rigid-ion or shell models. It has been successfully used to investigate the vibrational properties and infrared and Raman response of a large variety of binary and ternary $Al_xGa_{1-x}As$ superperiodic systems.[5,11,12] Details about the BCM parameters (only six) and its implementation for superperiodic heterostructures have been given elsewhere.[11,12] The most severe limitation of the present set of BCM parameters is in fact the relatively poor description of the longitudinal- (LO) and transverse- (TO) optical bulk dispersion relations of AlAs along the [001] direction: the calculations turn out in a too large bandwidth

when calculated within the mass approximation in comparison to first-principles calculations,[8] and a too low LO frequency at Γ if compared to experimental data.[13] Considering this observation, in the present paper we will focus mainly on the GaAs-like optical response. Consequently, we cannot comment about the reliability of the BCM in the AlAs spectral region of a GaAs/AlAs (113)-oriented SL. On the other hand, we remark that a discussion of the AlAs-like phonon modes would lead to similar results.

In Fig. 1(a) we show the crystal structure as seen along the [113] direction. The bulk primitive vectors $\{\mathbf{a}_i\}$ $(i=1,2,3)$ are chosen for further convenience such that

$$\mathbf{a}_1\cdot\hat{\boldsymbol{\eta}}=\mathbf{a}_2\cdot\hat{\boldsymbol{\eta}}=0,\quad \mathbf{a}_3\cdot\hat{\boldsymbol{\eta}}\neq 0\ , \tag{1}$$

where $\hat{\boldsymbol{\eta}}=(1/\sqrt{11},1/\sqrt{11},3/\sqrt{11})$ is the unit vector along the [113] axis. The reciprocal basis $\{\mathbf{b}_i\}$ is generated in the standard way with $\mathbf{b}_3$ parallel to $\hat{\boldsymbol{\eta}}$ and the resulting bulk BZ is the rectangular prism shown in Fig. 1(b). The $Z=(\pi/a)(113)$ point which lies at the zone boundary along the [113] direction in the bulk is equivalent in its symmetry to the L point of the fcc BZ.

The GaAs bulk phonon dispersion relations along the ΓZ direction are shown in Fig. 2(a). Thanks to the low-symmetry character of this direction, the degeneracy of the transverse vibrations is removed. Moreover, just two phonon branches have a pure transverse character [they have $[1\bar{1}0]$ polarization, and are indicated by dashed lines in Fig. 2(a)], while the remaining ones have mixed-longitudinal [113] mixed-transverse $[33\bar{2}]$ polarization. Incidentally, we remark that this is generally true for any $[11n]$ direction other than [111]. This feature is clearly shown by defining the character $S_\eta(j,\mathbf{q})$ of a vibrational mode (j is the branch index, $\mathbf{q}$ is the phonon wave vector) with respect to an arbitrary direction $\hat{\boldsymbol{\eta}}$ as

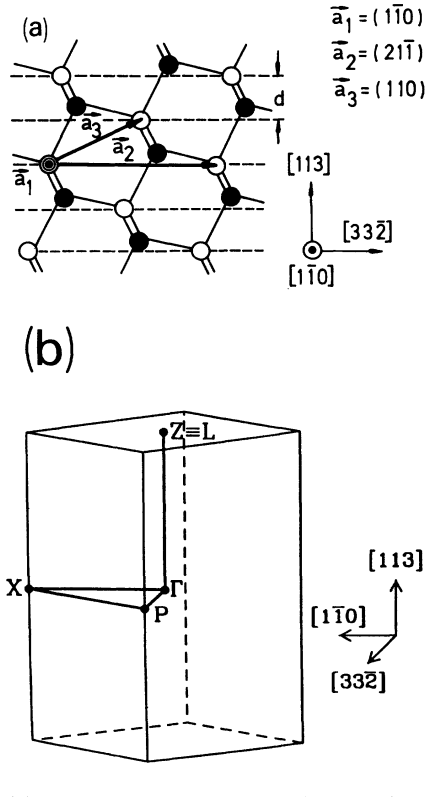

FIG. 1. (a) Crystal structure as seen along the [113] direction. $\{\mathbf{a}_i\}$ $(i=1,2,3)$ with $\mathbf{a}_1,\mathbf{a}_2\perp[113]$ is the bulk primitive vector basis. $d=a/\sqrt{11}$ is the thickness of a (113) monolayer. (b) [113]-adapted bulk Brillouin zone. The $Z=(\pi/a)(113)$ is symmetry equivalent to the L point of the conventional fcc BZ. The other high-symmetry points are: $X=(\pi/a)(1\bar{1}0)$ and $P=(\pi/a)(3/11,3/11,2/11)$.

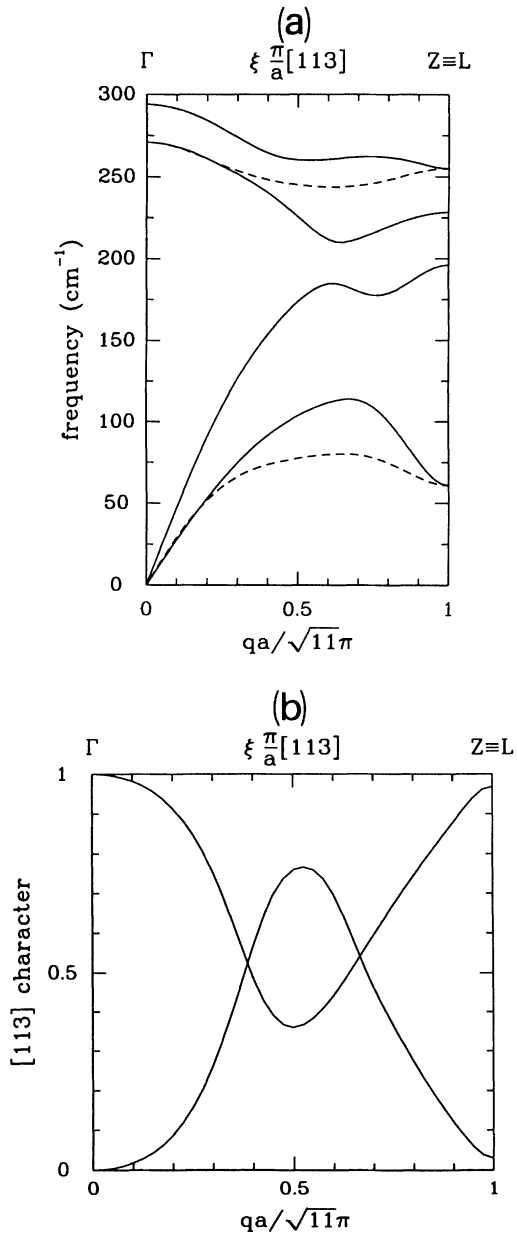

FIG. 2. (a) Bulk phonon dispersion relations of GaAs along the [113] direction. Full (dashed) lines represent mixed-character (pure-transverse) vibrations. (b) Phonon character plot for the two coupled longitudinal- and transverse-optical branches as defined in Eq. (2).

$$S_\eta(j,\mathbf{q})=\sum_{l\kappa}|\hat{\eta}\cdot\mathbf{e}(l\kappa|j\mathbf{q})|^2\ , \tag{2}$$

where $\mathbf{e}(lk|j\mathbf{q})$ is the eigenvector of the BCM dynamical matrix relative to the atom κ in the lth cell. The plot of the character for the two coupled longitudinal-transverse-optical branches is shown in Fig. 2(b): the mixed polarization is displayed everywhere except at the Γ point. The modes at the Z point are actually uncoupled in a basis oriented along the $[11\bar{1}]$ direction. The sign of the mixing [not appearing in Eq. (2)] is different for the two branches. It is worth noticing that the main component of the polarization is even reversed between the originally pure-longitudinal and pure-transverse modes when $\mathbf{q}$ lies midway to the ΓZ direction. Even more, the two character curves of Fig. 2(b) are not perfectly symmetric with respect to the 0.5 value. This feature is due to a coupling with acoustic phonons (which, in turn, display a similar behavior).

The polarization mixing and the assignment of the main character of a mode still remain valid in the superperiodic configuration for the confined modes originated by these bulk vibrations. As discussed in the following, this has relevant consequences in the SL dynamics.

B. Supercell calculations for SL's

In this section, we briefly describe our supercell (SC) approach to compute the dynamical matrix of a superperiodic system. The present SC scheme[14] is developed in the framework of the mass approximation where the same interatomic forces are assumed for both GaAs and AlAs layers.[5,8]

Let us consider a crystal lattice with primitive vectors $\{\mathbf{a}_1,\mathbf{a}_2,\mathbf{a}_3\}$ containing s atoms in the unit cell. The BZ is thus determined by a set of reciprocal vectors $\{\mathbf{b}_1,\mathbf{b}_2,\mathbf{b}_3\}$ such that $\mathbf{a}_i\cdot\mathbf{b}_j=2\pi\delta_{ij}$. If the original unit cell is enlarged M_1,M_2,M_3 times along $\mathbf{a}_1,\mathbf{a}_2,\mathbf{a}_3$, respectively, the extended cell can be constructed by the set of vectors $\{M_1\mathbf{a}_1,M_2\mathbf{a}_2,M_3\mathbf{a}_3\}$ and it will contain $M_1M_2M_3$ s atoms. The reciprocal vectors are consequently $\{\mathbf{B}_1,\mathbf{B}_2,\mathbf{B}_3\}=\{\mathbf{b}_1/M_1,\mathbf{b}_2/M_2,\mathbf{b}_3/M_3\}$ and generate a reduced BZ (RBZ) which is $M_1M_2M_3$ times smaller than the original one (OBZ).

The Fourier-transformed force constants (FC's) of the original lattice

$$\phi_{\alpha\beta}(\mathbf{q}|\kappa\kappa')=\sum_{l_1l_2l_3}\phi_{\alpha\beta}(l_1\mathbf{a}_1,l_2\mathbf{a}_2,l_3\mathbf{a}_3|\kappa\kappa')\times\exp\{i2\pi\mathbf{q}\cdot[l_1\mathbf{a}_1+l_2\mathbf{a}_2+l_3\mathbf{a}_3+\mathbf{x}(\kappa')-\mathbf{x}(\kappa)]\} \tag{3}$$

(here $\mathbf{q}$ belongs to OBZ) can be now more suitably cast in the following form:

$$\begin{aligned}\tilde{\phi}_{\alpha\beta}(\mathbf{Q}|\tilde{\kappa}\tilde{\kappa}')&=\sum_{L_1L_2L_3}\tilde{\phi}_{\alpha\beta}(L_1(M_1\mathbf{a}_1),L_2(M_2\mathbf{a}_2),L_3(M_3\mathbf{a}_3)|\tilde{\kappa}\tilde{\kappa}')\exp\{i2\pi\mathbf{Q}\cdot[L_1M_1\mathbf{a}_1+L_2M_2\mathbf{a}_2+L_3M_3\mathbf{a}_3+\mathbf{x}(\kappa')-\mathbf{x}(\kappa)]\}) \\ &=\sum_{L_1L_2L_3}\phi_{\alpha\beta}((L_1M_1+J_1'-J_1)\mathbf{a}_1,(L_2M_2+J_2'-J_2)\mathbf{a}_2,(L_3M_3+J_3'-J_3)\mathbf{a}_3,|\kappa\kappa') \\ &\quad\times\exp\{i2\pi\mathbf{Q}\cdot[(L_1M_1+J_1'-J_1)\mathbf{a}_1+(L_2M_2+J_2'-J_2)\mathbf{a}_2+(L_3M_3+J_3'-J_3)\mathbf{a}_3 \\ &\quad+\mathbf{x}(\kappa')-\mathbf{x}(\kappa)]\}\ ,\end{aligned} \tag{4}$$

where $\mathbf{q}$ spans the OBZ with a mesh of $(N_1/M_1)(N_2/M_2)(N_3/M_3)$ points (Born–von Karman conditions are used) and $\mathbf{Q}$ lies in the RBZ. Within the large unit cell, labeled by the set $\{L_1,L_2,L_3\}$, the atomic position $\tilde{\kappa}=(\mathbf{J},\kappa)$ is determined by $\mathbf{x}(\tilde{\kappa})=J_1\mathbf{a}_1+J_2\mathbf{a}_2+J_3\mathbf{a}_3+\mathbf{x}(\kappa)$, with $0\le J_i\le M_i-1$, $i=1,2,3$. Since the force constants for a given pair of atoms must be the same in both the original and extended-cell case (so far we have simply changed the basis of the lattice), i.e., $\tilde{\phi}_{\alpha\beta}=\phi_{\alpha\beta}$, we can substitute the back Fourier-transformed force constants of the original lattice into Eq. (4) and obtain

$$\begin{aligned}\tilde{\phi}_{\alpha\beta}(\mathbf{Q}|(\mathbf{J}\kappa)(\mathbf{J}'\kappa'))&=\sum_{\mathbf{q}}^{\mathrm{OBZ}}\phi_{\alpha\beta}(\mathbf{q}|\kappa\kappa')\exp\{i2\pi(\mathbf{Q}-\mathbf{q})\cdot[(J_1'-J_1)\mathbf{a}_1+(J_2'-J_2)\mathbf{a}_2+(J_3'-J_3)\mathbf{a}_3+\mathbf{x}(\kappa')-\mathbf{x}(\kappa)]\}\frac{1}{M_1M_2M_3} \\ &\quad\times\sum_{L_1,L_2,L_3}\frac{M_1M_2M_3}{N_1N_2N_3}\exp\{i2\pi(\mathbf{Q}-\mathbf{q})\cdot[L_1M_1\mathbf{a}_1+L_2M_2\mathbf{a}_2+L_3M_3\mathbf{a}_3]\} \\ &=\frac{1}{M_1M_2M_3}\sum_{\mathbf{G}}^{(\mathbf{Q}-G)\in\mathrm{OBZ}}\phi_{\alpha\beta}(\mathbf{Q}-\mathbf{G}|\kappa\kappa')\exp\{i2\pi\mathbf{G}\cdot[(J_1'-J_1)\mathbf{a}_1+(J_2'-J_2)\mathbf{a}_2 \\ &\quad+(J_3'-J_3)\mathbf{a}_3+\mathbf{x}(\kappa')-\mathbf{x}(\kappa)]\}\ ,\end{aligned} \tag{5}$$

where

$$\mathbf{G}=m_1\mathbf{B}_1+m_2\mathbf{B}_2+m_3\mathbf{B}_3=\frac{m_1}{M_1}\mathbf{b}_1+\frac{m_2}{M_2}\mathbf{b}_2+\frac{m_3}{M_3}\mathbf{b}_3$$

is the generic reciprocal vector of the RBZ and it is chosen in such a way that it maps the OBZ. As for Coulomb interactions, they are numerically computed by standard Ewald summations.

Equation (5) gives us the recipe to construct the SL dynamical matrix. Starting from the basis given in Eq. (1), we obtain the FC matrix for a (113) GaAs/AlAs SL making $M_1=M_2=1$ and $M_3=n_1+n_2$ and using bulk GaAs-like BCM force constants to calculate the $\phi_{\alpha\beta}(\mathbf{q}|\kappa\kappa')$ terms of Eq. (5). The dynamical difference between GaAs and AlAs is contained in the mass matrix. The validity of such a mass approximation has been demonstrated by first-principles calculations for (001) GaAs/AlAs SL's (Ref. 8) and successfully applied in several model calculations.[15]

Finally, we remark that the SL BZ is obtained from the bulk one by unfolding $M_3=n_1+n_2$ times along the ΓZ direction [see Fig. 1(b)].

C. Phonons in (113) SL's

Following the SC approach described in the preceding section, we have calculated the phonon-dispersion relations of two ultrathin superlattices with $n_1=n_2=3$ and $n_1=n_2=5$ along the Γ-P-X-Γ-Z directions [see Fig. 1(b)]. They contain 12 and 20 atoms, respectively, in the SL unit cell. Results are shown in Figs. 3(a) ($n_1=n_2=3$) and Fig. 3(b) ($n_1=n_2=5$).

As for the growth direction ΓZ (right panel), we found the well-known folding of the acoustic phonons caused by the reduction of the bulk BZ.[1] In particular, we can clearly observe the presence of several crossings and anticrossings (sometimes referred to as "phonon stop bands") among the phonon branches in both superlattices. They indicate that the two merging vibrational modes are decoupled and coupled, respectively. In other words, two phonon branches cannot interact when the symmetry of the related vibrations is different.

The high-frequency region shows two distinct bands for $210<\omega<280$ cm^{-1} and $320<\omega<380$ cm^{-1} corresponding to optical phonons confined in the GaAs and AlAs layers, respectively. In the case of the $(GaAs)_3/(AlAs)_3$ SL, several modes lying in the frequency region of both GaAs-like and AlAs-like optical vibrations show a sizable bandwidth that is strongly reduced in the thicker superlattice. This feature indicates that, to some extent, propagation of GaAs-like phonons takes place through the AlAs slab and vice versa. In other words, a (113)-oriented three-layer-thick SL turns out to be not very efficient to confine optical vibrations. This agrees with the fact that a three-monolayer-thick (113)-oriented layer is actually thinner than a two-monolayer-thick (001)-oriented one. The AlAs-like optical band still deserves a final comment. As mentioned above (see Sec. II), we have to recall that the reliability of the BCM in the mass approximation is questionable for the AlAs optical dispersions and, therefore, the total width of the 320 cm$^{-1}<\omega<380$ cm^{-1} band could be overestimated.

We now turn to the in-plane dispersions (i.e., $\mathbf{q}\perp[113]$) illustrated in the left panels of Figs. 3(a) and 3(b). Besides the anticrossing behavior that is clearly observed throughout the whole Brillouin zone, we note that, by increasing the thickness of the SL, the optical branches tend to merge into continuous bands of confined modes.[5]

In Fig. 4(a) we show the angular dispersion of high-frequency GaAs-like optical phonons for the 3/3 SL as obtained by rotating the phonon wave vector with $\mathbf{q}\sim 0$ in a fixed plane (indicated in the picture). The angular

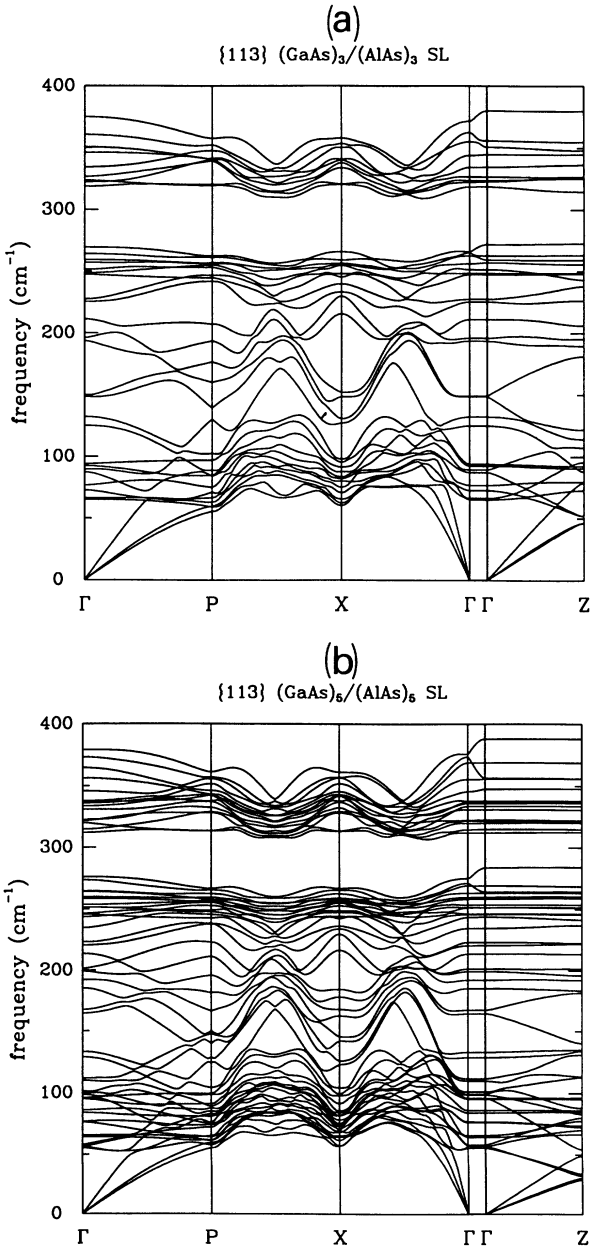

FIG. 3. (a) Phonon dispersion relations for the (113) $(GaAs)_3/(AlAs)_3$ SL. The Γ-Γ panel shows the angular dispersion (see text). (b) The same as in Fig. 3(a) for the (113) $(GaAs)_5/(AlAs)_5$ SL.

dispersion of optical phonons is a well-known property of uniaxial systems: it is related to the anisotropy of the macroscopic electric field associated to such vibrations. It has been experimentally obtained[6] and theoretically modeled in the context of a microscopic model for (001) GaAs/AlAs SL's.[5] However, the (113) case presents some interesting features as can be seen by comparing Fig. 4(a) with the angular dispersion calculated for a (001)-oriented 3/3 SL [see Fig. 4(b)]. First of all, the maximum vibrational frequency for the GaAs layer occurs at a wave vector that does not lie along the [113] direction. This is clearly seen in Fig. 4(a) where a $\omega \sim 273$ cm^{-1} phonon is observed when $\mathbf{q}$ is rotated in the $(1\bar{1}0)$ plane. The origin of this feature is related to the polarization mixing: the mode at 273 cm^{-1} with a wave vector lying along the $[113]$-$[\bar{3}\,\bar{3}2]$ direction turns out to have a more longitudinal character than the zone-center one. The latter, due to the folding of the bulk BZ, corresponds actually to a bulk phonon with a finite wave vector and, according to Fig. 2(b), has a nonpure longitudinal polarization. On the contrary, in (001)-oriented SL's, the maximum frequency at Γ occurs for $\mathbf{q}$ parallel to the growth direction. This feature is less evident for the thicker (113) superlattices: because of the larger superperiodicity, the SL zone-center phonon corresponds to a bulk mode with a smaller wave vector and stronger [113]-longitudinal character [see Fig. 2(b)].

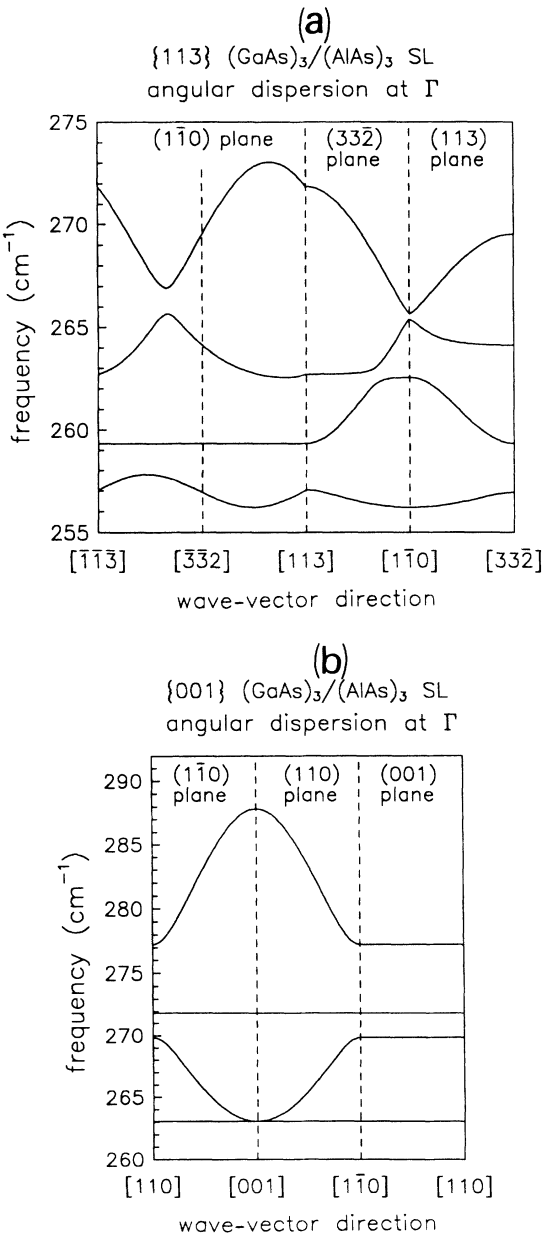

FIG. 4. (a) Angular dispersion for the high-frequency GaAs-like vibrations in the (113) $(GaAs)_3/(AlAs)_3$ SL. (b) The same as in Fig. 4(a) for the (001) $(GaAs)_3/(AlAs)_3$ SL.

Finally, we observe that for (001) SL's, the even m modes are dispersionless [as shown, for instance by the LO_2 mode at 271.9 cm^{-1} in Fig. 4(b)]. On the other hand, transverse modes vibrating along the $[1\bar{1}0]$ and $[110]$ directions remain uncoupled when $\mathbf{q}$ lies in the $(1\bar{1}0)$ and (110) plane, respectively. Consequently, they do not show angular dispersion (see TO_1, vibration at 263.1 cm^{-1}). Moreover, in (001) SL's, dispersion in the growth plane does not occur [see right panel of Fig. 4(b)]. On the contrary, in the high-frequency region of (113) SL's only that phonon vibrating along the $[1\bar{1}0]$ direction is dispersionless in the $(1\bar{1}0)$ plane. The other modes interact and anticrossings take place in the ω versus $\mathbf{q}$ plot. In-plane dispersion is actually obtained in our calculations for (113) SL's [right panel of Fig. 4(a)]. For $n_1, n_2 \to \infty$ this feature disappears.

III. RAMAN RESPONSE

A. The bond polarizability model for arbitrarily oriented SL

In order to calculate the Raman intensity for different polarizations we make use of the bond polarizability model that allows for the calculation of the scattering intensity of optical modes.[9] The BPM has been formerly used in the case of (001)-oriented SL's:[1,15,16] in the following we present an extension to an arbitrarily oriented superlattice.

In the spirit of the BPM, the polarizability of the whole crystal is calculated as a sum of independent contributions from each bond. Consequently, the variation $\Delta\chi_{\eta\chi}(j\mathbf{q})$ of the $\beta\gamma$ component of the polarizability tensor $\overleftrightarrow{\chi}$ due to a phonon mode j with wave vector $\mathbf{q}$ is given, for a zinc-blende lattice, by

$$\Delta\chi_{\beta\gamma}(j\mathbf{q}) = \sum_{l} \sum_{i=1}^{4} \Delta\chi_{\beta\gamma}(li|j\mathbf{q}) , \tag{6}$$

where $\Delta\chi_{\beta\gamma}(li|j\mathbf{q})$ is the variation of the polarizability of the ith bond of the lth cell. Then, the Raman intensity in the $\beta\gamma$ polarization for backscattering geometry [$\mathbf{q}\perp(\beta\gamma)$ plane and $\mathbf{q}\sim 0$] is given by

$$I_{\beta\gamma} \propto [n(\omega)+1] \sum_{j} \frac{\epsilon/\omega}{[\omega-\omega_j(\mathbf{q})]^2+\epsilon^2} |\Delta\chi_{\beta\gamma}(j\mathbf{q})|^2 , \tag{7}$$

where $[n(\omega)+1]$ is the Bose-Einstein population factor

for Stokes scattering and ϵ is a phenomenological broadening parameter. Neither Fröhlich interactions nor electro-optic effect are included in the model.

One has to calculate the $\Delta\vec{\chi}(li|j\mathbf{q})$ term of Eq. (6). Let $\{\hat{\mathbf{r}},\hat{\mathbf{s}},\hat{\mathbf{t}}\}$ be an orthonormal bond-oriented basis with $\hat{\mathbf{r}}$ parallel to the (li) bond. The bond polarizability $\vec{\chi}(li)$ is a diagonal tensor when expressed with respect to the bond-oriented basis. Its diagonal components are $(\alpha_\parallel,\alpha_\perp,\alpha_\perp)$, respectively, where $\alpha_\parallel$ and $\alpha_\perp$ are the parallel-to-bond and normal-to-bond polarizability. We can explicitly cast $\vec{\chi}$ in the following way:[9]

$$\vec{\chi}=\begin{bmatrix}\alpha_\parallel & 0 & 0\\ 0 & \alpha_\perp & 0\\ 0 & 0 & \alpha_\perp\end{bmatrix}=\alpha_0\overleftrightarrow{1}+\alpha_2\begin{bmatrix}2 & 0 & 0\\ 0 & \bar{1} & 0\\ 0 & 0 & \bar{1}\end{bmatrix}, \tag{8}$$

where $\overleftrightarrow{1}$ is the unit matrix. We have introduced two new parameters in Eq. (8):

$$\alpha_0=\tfrac{1}{3}(\alpha_\parallel+2\alpha_\perp),\quad \alpha_2=\tfrac{1}{2}(\alpha_\parallel-\alpha_\perp)\ . \tag{9}$$

To the linear order in the variation $\Delta\lambda$ of the bond length, we can assume that $\Delta\alpha=\alpha'\Delta\lambda$ ($\Delta\alpha$ denotes the variation of the bond polarizability and $\alpha'=d\alpha/d\lambda$). The susceptibility $\vec{\chi}(li)$ and the corresponding $\Delta\vec{\chi}(li)$ can be written, in a general basis $\{\hat{\mathbf{x}},\hat{\mathbf{y}},\hat{\mathbf{z}}\}$, as

$$\vec{\chi}(li)=\alpha_0(l)\overleftrightarrow{1}+\alpha_2(l)A_1(i)\ , \tag{10a}$$

$$\begin{aligned}\Delta\vec{\chi}(li)=&[\mathbf{u}(li|j\mathbf{q})\cdot\hat{\mathbf{r}}(i)][\alpha_0'(l)\overleftrightarrow{1}+\alpha_2'(l)A_1(i)]\\ &+\frac{3\alpha_2(l)}{\lambda}[\mathbf{u}(li|j\mathbf{q})\cdot\hat{\mathbf{s}}(i)]A_2(i)\\ &+\frac{3\alpha_2(l)}{\lambda}[\mathbf{u}(li|j\mathbf{q})\cdot\hat{\mathbf{t}}(i)]A_3(i)\ ,\end{aligned} \tag{10b}$$

where the prime indicates the derivative with respect to the bond length λ and $\mathbf{u}(li|j\mathbf{q})$ is the *relative* displacement of the atoms forming the ith bond in the lth cell. The matrices $A_\sigma(i)$, $\sigma=1,2,3$, are defined as follows:

$$\begin{aligned}A_1(i)&=C^{-1}(i)\begin{bmatrix}2 & 0 & 0\\ 0 & \bar{1} & 0\\ 0 & 0 & \bar{1}\end{bmatrix}C(i)\ ,\\ A_2(i)&=C^{-1}(i)\begin{bmatrix}0 & 1 & 0\\ 1 & 0 & 0\\ 0 & 0 & 0\end{bmatrix}C(i)\ ,\\ A_3(i)&=C^{-1}(i)\begin{bmatrix}0 & 0 & 1\\ 0 & 0 & 0\\ 1 & 0 & 0\end{bmatrix}C(i)\ ,\end{aligned} \tag{11}$$

where $C(i)$ is the rotation matrix from $\{\hat{\mathbf{x}},\hat{\mathbf{y}},\hat{\mathbf{z}}\}$ to the bond-oriented $\{\hat{\mathbf{r}}(i),\hat{\mathbf{s}}(i),\hat{\mathbf{t}}(i)\}$ basis. In Eqs. (10) and (11) we have made use of the fact that for unstrained structures neither $\hat{\mathbf{r}},\hat{\mathbf{s}},\hat{\mathbf{t}}$ nor $C(i)$ depends on the cell index l. Moreover, for common anion systems like the GaAs/AlAs SL's, investigated here both the parallel-to-bond and the normal-to-bond polarizability do not depend on either the bond index i, or their derivatives.

The equation for $\Delta\vec{\chi}(li)$ as expressed in Eq. (10b) can be applied to an arbitrary supercell (see Sec. II B). In the specific case of (113)-grown SL's, we just need to take $\{\hat{\mathbf{x}},\hat{\mathbf{y}},\hat{\mathbf{z}}\}=\{1/\sqrt{2}(1\bar{1}0),1/\sqrt{22}(33\bar{2}),1/\sqrt{11}(113)\}$: explicit calculations are carried out in Appendix A. There we show that we have only four different parameters to determine [see Eqs. (A3)–(A13)]: α_b(GaAs), α_b(AlAs), α_0'(GaAs)-α_0'(AlAs), and α_2(GaAs)/$\lambda-\alpha_2$(AlAs)/λ, where we have introduced the compact notation: $\alpha_b(l)=\alpha_2'(l)-2\alpha_2/\lambda$. As for the bulk parameters α_b(GaAs), α_b(AlAs), they are equivalent to the xy component of the bond polarizability in the (001) case; according to Refs. 12, 15, and 16 we put α_b(GaAs)$=3\alpha_b$(AlAs). The other two parameters are nonzero only at the interface: the contribution of the tensity is negligible for long-period superlattices and for high-order confined phonons in short-period ones. In the present paper we have assumed that $\alpha_2/\lambda\ll\alpha_0'$, $\alpha_\perp'\ll\alpha_\parallel'$, and α_2(GaAs)/$\lambda>\alpha_2$(AlAs)/λ.[17] In particular, we have taken

$$\begin{aligned}\alpha_0'(\text{GaAs})-\alpha_0'(\text{AlAs})&=15\left[\frac{\alpha_2(\text{GaAs})}{\lambda}-\frac{\alpha_2(\text{AlAs})}{\lambda}\right]\\ &=3\alpha_b(\text{AlAs})=\alpha_b(\text{GaAs})\end{aligned}$$

and we have checked that reasonable variations of such parameters do not induce major changes in the calculated Raman spectra.

B. Raman spectra of short-period (113) SL's

In Figs. 5 and 6 (solid line) we show the intensity of the Raman scattering calculated in the GaAs-like region for

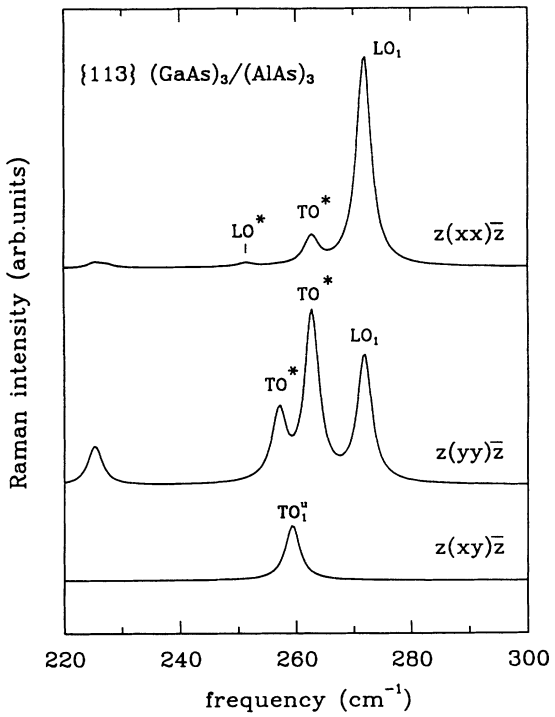

FIG. 5. Calculated Raman spectrum of the (113) $(GaAs)_3/(AlAs)_3$ SL with ideal interfaces (i.e., no cationic intermixing) for three different polarizations. Main peaks are labeled according to the discussion reported in the text.

the 3/3 and 5/5 SL's, respectively, using the model described in the previous section. The backscattering geometry and three polarizations $z(xx)\bar{z}$, $z(yy)\bar{z}$, and $z(xy)\bar{z}$ have been considered. Ideal interfaces without cationic intermixing are assumed (dashed line spectra of Fig. 6 including the interface disorder will be discussed in the next section). Each Raman-active phonon mode is labeled according to its dominant character and its displacement pattern (order).

Let us consider the top $z(xx)\bar{z}$ and center $z(yy)\bar{z}$ spectra where only modes normal to the $[1\bar{1}0]$ direction are allowed (see Appendix A). They correspond to $[113]\pm[33\bar{2}]$ coupling. The LO_1-like peak, located at 272 and 284 cm^{-1} for the 3/3 and 5/5 SL respectively, has a nonpure-longitudinal [113] character with a small but not negligible $[\bar{3}\,\bar{3}2]$ component. The mixed character causes the intensity ratio between the $z(xx)\bar{z}$ and $z(yy)\bar{z}$ spectra to be quite different from the corresponding $I_{xx}(LO)/I_{yy}(LO)=4.84$ one, as calculated for pure [113] modes (see Appendix B). In fact, this ratio is 1.7 for the 3/3 SL and 2.9 for the 5/5 SL showing a tendency to the bulk value for the thicker superlattice: the larger the SL period, the lower the mixed character.

Two mainly TO peaks (labeled TO*) are the more striking features of the center spectrum in both Figs. 5 and 6. These modes have a strong mixed character originated by a coupling between TO and LO phonons. Their envelope functions (not shown here) do not have a simple sinusoidal shape: however, it is possible to resolve them as a superposition of a $[33\bar{2}]$-like TO_1 mode and a [113]-like LO_2 vibration. The interference between the [113]-like and the $[33\bar{2}]$-like contributions is constructive for the LO_1 mode and destructive for the TO* modes. This interference effect[18] is responsible for the vanishing intensity of the phonon at 257 cm^{-1} in the $z(xx)\bar{z}$ polarization for the 3/3 SL (see Fig. 5).

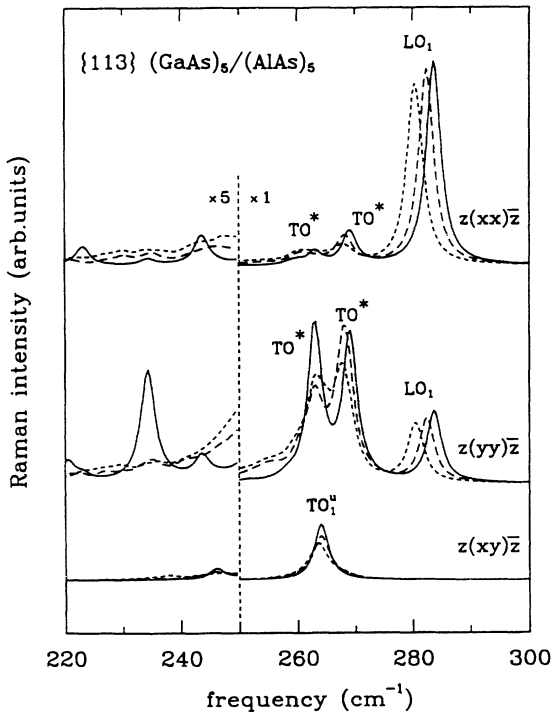

FIG. 6. Solid line: the same as in Fig. 5 for the (113) $(GaAs)_5/(AlAs)_5$ SL. Calculated Raman spectra of the (113) $(GaAs)_5/(AlAs)_5$ including interface disorder: short-dashed line, the interface region has been chosen two monolayers thick with 66% and 33% Al content, respectively; long-dashed line: the interface regions consist of only one monolayer with a nominal 50% composition.

In the low-frequency region of the spectra shown in Figs. 5 and 6 we can observe delocalized phonons whose displacement patterns (not shown here) display a nonzero vibrational amplitude at the interfaces. The spectral features falling into this region show a sizable dependence upon the $\alpha_0'(GaAs)-\alpha_0'(AlAs)$ and $\alpha_2(GaAs)/\lambda - \alpha_2(AlAs)/\lambda$ parameters: however, this dependence is strongly reduced by the interface disorder due to cation intermixing (see the next section).

As for the Raman spectrum calculated in the $z(xy)\bar{z}$ geometry (bottom spectrum of Figs. 5 and 6), only the $[1\bar{1}0]$ pure-transverse uncoupled modes can be observed. However, their intensity is considerably reduced with respect to that of the $z(xx)\bar{z}$ and $z(yy)\bar{z}$ cases and, consequently, only the first TO phonon has a sizeable contribution (here labeled as TO_1^u). The small peak close to 246 cm^{-1} for the 5/5 SL is related to the TO_3^u phonon.

We would like to comment on the validity of the standard equivalent wave vector rule (EWR).[1] Following the EWR, the frequency and the character of a mode confined in the layer A correspond to those of a bulk phonon with a wave vector given by[4]

$$q_m=\frac{m\pi}{(n_A+\xi)d}\ , \tag{12}$$

where d is the monolayer thickness, n_A the number of monolayers of material A, and $m=1,2,\ldots,n_A$ is the order of the confined phonon. ξ is an orientation-dependent effective parameter which is found to be $\xi=1$ for (001)-oriented SL's.[1]

For the uncoupled TO_m^u modes in (113) SL's, Eq. (12) is still valid even for the ultrathin 3/3 and 5/5 cases and the best choice is $\xi=1$. On the other hand, for the LO_1 modes, the EWR is qualitatively fulfilled; however, a simultaneous quantitative agreement for both the mode frequency and mode character cannot be found. Finally, for the TO*-like modes, the EWR fails due to the strong mode mixing occurring in the short-period SL's. For low-frequency optical modes both in the 3/3 and 5/5 systems, we cannot apply Eq. (12) due to the fact that they are almost not confined.

C. Interface disorder

So far we have considered SL's with ideal interfaces. This means that we have neglected any cationic intermixing which very likely takes place during the growth process. In fact, for (001)-oriented SL's the interface disorder due to cationic diffusion is known to have important consequences in the vibrational properties of ultrathin su-

perlattices and Raman spectroscopy has been used to investigate the interface quality.[19] Moreover, according to recent experimental results,[20] the interface disorder in (113) heterostructures has been found to be larger than in (001) ones. Consequently, a theoretical modeling of the dynamical effects of disorder is needed.

In Fig. 6 we have calculated the Raman spectrum of the $(GaAs)_5/(AlAs)_5$ system assuming two different modelings of interface disorder: (i) the interface region has been chosen as thick as two monolayers with 66% and 33% Al content (short dashed line); (ii) the interface region consists of only one monolayer with a nominal 50% composition (long dashed line).

The interface alloying has been modeled within the present SC mass approximation without using any mean-field approach (such as average t-matrix approximation or coherent potential approximation). By means of the formalism developed in Sec. II B, we have built a supercell as thick as the superperiodic constant along the (113) direction and large enough to contain 16 atoms in the planes normal to it. The resulting SC contains 320 atoms. In the interface planes, Ga and Al atoms have been distributed at random with a relative abundance corresponding to the desired composition. In order to rule out statistical fluctuations in our spectra, configurational averages have been evaluated over four different spectra corresponding to different random distributions of cation masses at the interface planes and the Raman response has been calculated by means of Eq. (10b). Incidentally, we remark that a SC surface area containing 16 atoms for (113)-oriented SL's corresponds to a SC with 26 atoms on each plane for the (001) orientation.

As we can see by comparison with the ideal case (full line), the variations in the Raman response are always important. This is particularly evident for the middle spectra of Fig. 6 where the TO* peaks broaden and overlap. Moreover, a sizable shift towards lower frequencies is found for the LO_1 peak as can be very clearly seen in the $z(xx)\bar{z}$ spectra. This shift is related to the reduction of the effective GaAs thickness. Nevertheless, the intensity ratio $I_{xx}(LO_1)/I_{yy}(LO_1)$ remains almost constant. This feature cannot be accounted for by the EWR: according to Eq. (12) and Figs. 2(a) and 2(b), a frequency shift towards lower frequency should imply an appreciable increase of the character mixing and, therefore, a decrease of the $I_{xx}(LO_1)/I_{yy}(LO_1)$ intensity ratio. The peaks in the range 220–250 cm^{-1} are not clearly observable when cationic intermixing is present: consequently, a change in the interface-related $\alpha_0'(GaAs)-\alpha_0'(AlAs)$ and $\alpha_2(GaAs)/\lambda-\alpha_2(AlAs)/\lambda$ parameters does not affect the calculated spectra for SL's with interface disorder.

Finally, we have considered also a different way to model interface disorder. In particular, we have studied the case where Ga and Al atoms are not distributed at random, but are grouped to form small GaAs or AlAs islands into the interface region. A SC large enough to contain 35 atoms on each plane normal to the [113] direction was selected. The calculations were performed for the same *average* relative concentration of Al and Ga atoms that we considered in Fig. 6. The results are very similar to those discussed above and make us confident about the validity of our conclusions.

D. Long-period SL's: comparison to experimental results

The effects of interface disorder are less sizable in the case of thick SL's. Accordingly, we have extended our analysis to the $(GaAs)_{26}/(AlAs)_{26}$ SL where experimental data are available. The results of our calculation in the $z(xx)\bar{z}$ geometry are shown in Fig. 7. In this case, due to the long superlattice period which reduces the polarization mixing as discussed above, we can identify more easily the order of the most relevant phonon modes: according to Eq. (12) we have labeled those modes as LO_m and TO_m when their polarization is, respectively, mainly LO and mainly TO. Moreover, being the parity almost well defined in the long-period (113) SL's, the only important contributions to the calculated Raman intensity come from modes with odd m. Concerning the EWR, it is fulfilled by the main optical modes.

We have performed Raman measurements on a $(GaAs)_{26}(AlAs)_{26}$ SL. The experimental Raman spectrum is presented in Fig. 7 (top). The sample was grown by atomic layer molecular-beam epitaxy[21] on {113} GaAs substrate. The growth took place at low temperature ($T=350\,°C$) and no faceting of the surface was observed by reflection high-energy electron diffraction.[22] The light excitation source for the Raman measurements was the 752.4-nm line of a Kr^+ laser. The spectrum shown in Fig. 7 was taken at $T=100$ K, close to (but not at) resonant conditions.

Experimental LO_1, LO_3, LO_5, and TO_1 peaks have been labeled according to the theoretical spectrum (Fig. 7, bottom). Arrows correspond to the theoretical frequencies. We have also indicated the position of the LO_2

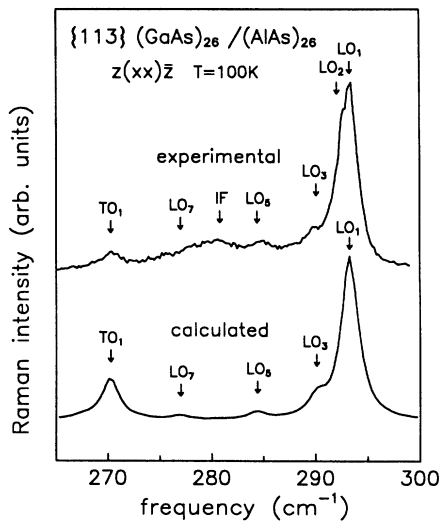

FIG. 7. Experimental (top) and calculated (bottom) Raman spectra for the (113) $(GaAs)_{26}/(AlAs)_{26}$ SL in the $z(xx)\bar{z}$ polarization. Black arrows indicate the relevant theoretical frequencies.

phonon which can be detected because of the Fröhlich mechanism (not included in the BPM). Evidence of a LO_7 vibration close to 277 cm^{-1} is found in the calculated spectrum , but such a structure was not experimentally resolved. The broad feature around 280 cm^{-1} is attributed to an electrostatic interface mode (IF).[4,23] This phonon mode has a wave vector perpendicular to the growth axis and can be observed because of scattering induced by interface roughness of defects.[23] The calculated frequency for the first IF mode ($\omega=280.5$ cm^{-1} and LO-like character) seems to confirm this attribution.

The agreement between experiment and theory is rather good, even though we have not taken into account the electro-optic effect which will imply different polarizabilities α for the LO and TO modes.

IV. CONCLUSIONS

We have presented a thorough theoretical investigation of the phonon spectrum of (113)-oriented GaAs/AlAs superlattices based on a reliable model calculation.

The lattice-dynamical properties of such heterostructures appear to be dominated by the polarization mixing of the phonon modes due to the low symmetry of the selected growth direction. In particular, unusual angular dispersions are displayed by the zone-center optical phonons. We have also studied the influence of mode mixing on the Raman scattering of optical phonons.

Moreover, we have shown that the interface disorder plays a major role in the Raman response of a short-period superlattice with nonideal interfaces.

Finally, rather good agreement is found between the present theoretical investigation and experimental data for long-period superlattices.

ACKNOWLEDGMENTS

One of us (L.C.) acknowledges financial support from the Italian Consiglio Nazionale delle Ricerche through the "Progetto Finalizzato Materiali Speciali per Tecnologie Avanzante." This work has been partially supported by the Spanish Comisión Interministerial de Ciencia y Tecnología under Project No. MAT92-0262.

TABLE I. Components of the $\Delta\vec{\vec{\chi}}$ tensor for a bulk zinc-blende crystal calculated with respect to the (113)-oriented basis [see Sec. III A and Fig. 1(a)]. Units of $[(4\sqrt{2}/\sqrt{33})\alpha_b u]$ are adopted. The mode polarization is also shown.

	xx	yy	xy
TO($1\bar{1}0$)	0	0	1
TO($33\bar{2}$)	1	$\frac{27}{11}$	0
LO(113)	$\frac{3}{\sqrt{2}}$	$\frac{15}{11\sqrt{2}}$	0

APPENDIX A

The key quantity to compute the Raman intensity as expressed in Eq. (7) is the variation $\Delta\vec{\vec{\chi}}(j\mathbf{q})$ of the susceptibility due to a phonon mode with branch index j and wave vector $\mathbf{q}$. If we expand $\Delta\vec{\vec{\chi}}(j\mathbf{q})$ up to the linear order in the atomic displacements $\mathbf{u}(l\kappa|j\mathbf{q})$ (where κ and l are the atom and bulk unit cell index, respectively) we can cast Eq. (6) in the following form:

$$\Delta\chi_{\beta\gamma}(j\mathbf{q})=\sum_{l\kappa\delta}\frac{\partial\chi_{\beta\gamma}}{\partial u_\delta}(l\kappa)u_\delta(l\kappa|j\mathbf{q})\ . \tag{A1}$$

We can now insert the above expression into Eq. (7) and obtain (in the limit of vanishing wave vector)

$$I_{\beta\gamma}\propto[n(\omega)+1]\sum_{l\kappa}\sum_{l'\kappa'}\sum_{\delta\delta'}\frac{\partial\chi_{\beta\gamma}}{\partial u_\delta}(l\kappa)\frac{\partial\chi_{\beta\gamma}}{\partial u_{\delta'}}(l'\kappa')\times\mathrm{Im}G_{\delta\delta'}\left[l\kappa,l'\kappa',\omega+i\frac{\epsilon}{2};\mathbf{q}\right]\ , \tag{A2}$$

where $\vec{\vec{G}}(l\kappa,l'\kappa',\omega;\mathbf{q})$ is the vibrational Green function of the SL for the phonon wave vector $\mathbf{q}$.[24] By comparing Eq. (10b) [where the $A_\sigma(i)$ are the suitable rotation matrices for the (113)-oriented SL] to Eq. (A3), we obtain

$$\frac{\partial\chi_{xx}}{\partial u_x}(l\kappa)=\frac{\partial\chi_{yy}}{\partial u_x}(l\kappa)=\frac{\partial\chi_{xy}}{\partial u_y}(l\kappa)=\frac{\partial\chi_{xy}}{\partial u_z}(l\kappa)=0\ , \tag{A3}$$

$$\frac{\partial\chi_{xx}}{\partial u_y}(l1)=-\frac{4\sqrt{2}}{\sqrt{33}}\alpha_b(l)\ , \tag{A4}$$

$$\frac{\partial\chi_{xx}}{\partial u_y}(l2)=\frac{2\sqrt{2}}{\sqrt{33}}\left\{\alpha_b(l+1)+2\alpha_b(l)-\alpha_b(l-1)+\alpha_0'(l+1)-2\alpha_0'(l)+\alpha_0'(l-1)-\frac{2}{\lambda}[\alpha_2(l+1)-2\alpha_2(l)+\alpha_2(l-1)]\right\}\ , \tag{A5}$$

$$\frac{\partial\chi_{xx}}{\partial u_z}(l1)=\frac{12}{\sqrt{33}}\alpha_b(l)\ , \tag{A6}$$

$$\frac{\partial\chi_{xx}}{\partial u_z}(l2)=-\frac{1}{\sqrt{33}}\left\{6\alpha_b(l+1)+\alpha_b(l)+5\alpha_b(l-1)+6\alpha_0'(l+1)-\alpha_0'(l)-5\alpha_0'(l-1)\right.$$
$$\left.-\frac{2}{\lambda}[6\alpha_2(l+1)-\alpha_2(l)-5\alpha_2(l-1)]\right\}, \tag{A7}$$

$$\frac{\partial\chi_{yy}}{\partial u_y}(l1)=\frac{108\sqrt{2}}{11\sqrt{33}}\alpha_b(l), \tag{A8}$$

$$\frac{\partial\chi_{yy}}{\partial u_y}(l2)=\frac{2\sqrt{2}}{\sqrt{33}}\left\{-\frac{3}{11}[3\alpha_b(l+1)+14\alpha_b(l)+\alpha_b(l-1)]+\alpha_0'(l+1)-2\alpha_0'(l)+\alpha_0'(l-1)\right.$$
$$\left.+\frac{4}{\lambda}[\alpha_2(l+1)-2\alpha_2(l)+\alpha_2(l-1)]\right\}, \tag{A9}$$

$$\frac{\partial\chi_{yy}}{\partial u_z}(l1)=-\frac{60}{11\sqrt{33}}\alpha_b(l), \tag{A10}$$

$$\frac{\partial\chi_{yy}}{\partial u_z}(l2)=\frac{1}{\sqrt{33}}\left\{\frac{3}{11}[18\alpha_b(l+1)+7\alpha_b(l)-5\alpha_b(l-1)]-6\alpha_0'(l+1)+\alpha_0'(l)+5\alpha_0'(l-1)\right.$$
$$\left.+\frac{2}{\lambda}[6\alpha_2(l+1)-\alpha_2(l)-5\alpha_2(l-1)]\right\}, \tag{A11}$$

$$\frac{\partial\chi_{xy}}{\partial u_x}(l1)=-4\sqrt{\tfrac{2}{33}}\alpha_b(l), \tag{A12}$$

$$\frac{\partial\chi_{xy}}{\partial u_x}(l2)=4\sqrt{\tfrac{2}{33}}\left\{\alpha_b(l+1)+\frac{6}{\lambda}[\alpha_2(l+1)-2\alpha_2(l)+\alpha_2(l-1)]\right\}. \tag{A13}$$

APPENDIX B

For bulk materials, the $\beta\gamma$ components of the $\Delta\vec{\vec{\chi}}$ tensor can be easily calculated for the three optical vibrations at Γ. They are listed in Table I.

Neglecting the Bose-Einstein prefactor in Eq. (7), we can compute the intensity ratios for the different scattering geometries as follows:

$$\frac{I_{xx}(\mathrm{LO})}{I_{yy}(\mathrm{LO})}=4.84,\quad \frac{I_{yy}(\mathrm{TO})}{I_{xx}(\mathrm{TO})}=6.02,$$
$$\frac{I_{xx}(\mathrm{LO})}{I_{xx}(\mathrm{TO})}=4.5,\quad \frac{I_{yy}(\mathrm{LO})}{I_{yy}(\mathrm{TO})}=6.48.$$

*Permanent address: Centro Nacional de Microelectrónica—CSIC—Serrano 144, 28006 Madrid, Spain.

[1]B. Jusserand and M. Cardona, in *Light Scattering in Solids V*, edited by M. Cardona and G. Güntherodt (Springer-Verlag, Heidelberg, 1989).
[2]Z. V. Popovic, M. Cardona, E. Richter, D. Strauch, L. Tapfer, and K. Ploog, Phys. Rev. B **40**, 1207 (1989).
[3]Z. V. Popovic, M. Cardona, E. Richter, D. Strauch, L. Tapfer, and K. Ploog, Phys. Rev. B **40**, 3040 (1989).
[4]Z. V. Popovic, M. Cardona, E. Richter, D. Strauch, L. Tapfer, and K. Ploog, Phys. Rev. B **43**, 4925 (1991).
[5]L. Miglio and L. Colombo, Surf. Sci. **221**, 486 (1989).
[6]G. Scamarcio, M. Haines, G. Abstreiter, E. Molinari, S. Baroni, A. Fischer, and K. Ploog, Phys. Rev. B **47**, 1483 (1993).
[7]W. Weber, Phys. Rev. B **15**, 4789 (1977); K. C. Rustagi and W. Weber, Solid State Commun. **18**, 673 (1976).
[8]P. Giannozzi, S. de Gironcoli, P. Pavone, and S. Baroni, Phys. Rev. B **43**, 7231 (1991).
[9]A. A. Maradudin and E. Burnstein, Phys. Rev. **164**, 1081 (1967).
[10]D. Strauch and B. Dorner, J. Phys. Condens. Matter **2**, 1457 (1990).
[11]M. Bernasconi, L. Colombo, L. Miglio, and G. Benedek, Phys. Rev. B **43**, 14 447 (1991); **43**, 14 457 (1991).
[12]L. Miglio, C. Molteni, and M. Bernasconi, Appl. Phys. Lett. **59**, 788 (1991); L. Colombo, C. Molteni, and L. Miglio, Superlatt. Microstruct. **12**, 523 (1992).
[13]A. Onton, in *Proceedings of the 10th International Conference on the Physics of Semiconductors*, edited by S. P. Keller, J. C. Heusel, and F. Stern (U.S. Atomic Energy Commision, New York, 1970), p. 107.
[14]L. Miglio and L. Colombo, Superlatt. Microstruct. **7**, 139 (1990).
[15]For a recent review, see C. Molteni, L. Colombo, L. Miglio, G. Benedek, and M. Bernasconi, Philos. Mag. B **65**, 325 (1992).
[16]A. S. Barker, J. L. Merz, and A. C. Gossard, Phys. Rev. B **17**,

3181 (1978).
[17]This is in reasonable agreement with the BPM parameters for the sequence C, Si, Ge. See M. Cardona, in *Light Scattering in Solids II,* edited by M. Cardona and G. Güntherodt (Springer-Verlag, Heidelberg, 1989), p. 67.
[18]J. Menéndez and M. Cardona, Phys. Rev. B **31**, 3696 (1985).
[19]B. Jusserand, F. Alexandre, D. Paquet, and G. Le Roux, Appl. Phys. Lett. **47**, 301 (1985).
[20]J. Meléndez, A. Mazuelas, P. S. Domínguez, M. Garriga, M. I. Alonso, G. Armelles, L. Tapfer, and F. Briones, Appl. Phys. Lett. **62**, 1000 (1993).
[21]F. Briones, L. González, and A. Ruiz, Appl. Phys. A **49**, 729 (1989).
[22]P. S. Domínguez (private communication).
[23]A. K. Sood, J. Menéndez, M. Cardona, and K. Ploog, Phys. Rev. Lett. **54**, 2115 (1985).
[24]A. A. Maradudin, E. W. Montroll, G. H. Weiss, and I. P. Ipatova, *Theory of Lattice Dynamics in the Harmonic Approximation,* 2nd ed. (Academic, New York, 1971), p. 66.